Chapter 6

Networks with compliant cross-links

Based on: G. Žagar, P.R. Onck and E. Van der Giessen, "*Two Fundamental Mechanisms Govern the Stiffening of Cross-linked Networks*", in preparation.

A random fibre network is an ubiquitous microstructure in many materials, ranging from metallic open cell foams through felts, paper and rubbers (Gibson and Ashby, 1997; Kabla and Mahadevan, 2007; Picu, 2011) to the scaffolds of biopolymer filaments in soft tissue and the cell cytoskeleton (Bausch and Kroy, 2006; Kasza et al., 2007; Lieleg et al., 2010; Lodish et al., 2000). While the mechanical behavior of these materials evidently depends on the constituents, the underlying network microstructure is particularly important at large strains. Numerous rheological experiments have shown that random fibre networks of *in vitro* reconstituted biopolymer networks exhibit strong nonlinear elastic strain-stiffening accompanied with an increase of the shear modulus up to three orders of magnitude (Gardel et al., 2004a,b; Shin et al., 2004; Wagner et al., 2006; Gardel et al., 2006; Tharmann et al., 2007; Lieleg et al., 2007; Kasza et al., 2009; Schmoller et al., 2009; Kang et al., 2009; Yao et al., 2010; Lindstrom et al., 2010; Vader et al., 2009; Orakdogen et al., 2010). Several synthetic polymer network systems show a similar phenomenology as biopolymer networks, albeit with a much weaker increase of the modulus up to a factor of $\sim$2 (Erk et al., 2010).

The strain-stiffening in biopolymer networks is, generally, attributed to the (i) properties of the fibres, (ii) the cross-links that mediate the inter-fibre force transmission and (iii) the network microstructure. In so far as the fibre constituent is concerned, the physics of individual biopolymer fibres, like actin filaments (F-actin), is generally well understood within the framework of a semi-flexible worm like chain model (Marko and Siggia, 1995; MacKintosh et al., 1995; Ghosh et al.,

2007; van Dillen et al., 2008; Holzapfel and Ogden, 2011). The cross-links found in biopolymers (Yamazaki et al., 2002; Guo and Guilford, 2006; Ferrer et al., 2008; Lee et al., 2009) however, have a diverse mechanical behavior. In addition, the cross-linking macromolecules that commonly interconnect biopolymer filaments at higher concentrations often tend to bundle the filaments into thicker fibres, thereby changing the network microstructure (Lieleg et al., 2007; Schmoller et al., 2009; Lieleg et al., 2009b).

6.1 Strain-stiffening revisited

Despite the differences in microstructure and/or properties of the constituents, the nonlinear stiffening of biopolymer networks shows quite similar trends, as shown in Figure 6.1. The stiffening of F-actin networks cross-linked by scruin (Gardel et al., 2004a,b) and that of cross-linked neuro-filaments (Lin et al., 2010b) can be characterised by a power-law relation with exponent 3/2 between the network shear modulus G and macroscopic stress T (Figure 6.1a). Since the cross-links in both these networks are relatively stiff, it has been suggested that the stiffening mechanism is the same (Storm et al., 2005; Žagar et al., 2011). However, F-actin networks cross-linked by heavy-meromyosin in a rigor state (rigor-HMM) (Tharmann et al., 2007), which are also considered as rigidly cross-linked, show a stiffening behavior with an exponent far less than 3/2 (Figure 6.1b). Moreover, the stiffening exponent in F-actin/rigor-HMM networks is found to decrease as the cross-link concentration increases, similar as in purely bundled F-actin networks cross-linked by fascin (Lieleg et al., 2007) (Figure 6.1c). On the other hand, F-actin networks cross-linked by the long flexible protein filamin (Gardel et al., 2006; Kasza et al., 2009) (Figure 6.1d) as well as rigidly cross-linked networks of the intermediate filament vimentin (Lin et al., 2010b,a) (Figure 6.1e) start to stiffen according to a 3/2 power law, but at higher stress the stiffening changes into a weaker power law. The exponent of the latter is remarkably similar to the exponents found in F-actin/rigor-HMM networks, as well as in branched collagen I type networks (Vader et al., 2009; Lindstrom et al., 2010) (Figure 6.1f). The aforementioned similarities in the large strain behavior of various cross-linked biopolymer networks hint at a generic behavior, where underlying physical mechanisms however, are not yet understood.

The objective in this chapter is to uncover the mechanisms behind this common behavior through a numerical study of the nonlinear response of random fibre networks subjected to simple shear. Periodic representative volume element (RVE) of a random fibre network in 3D is sefl-assembled by using the numerical method

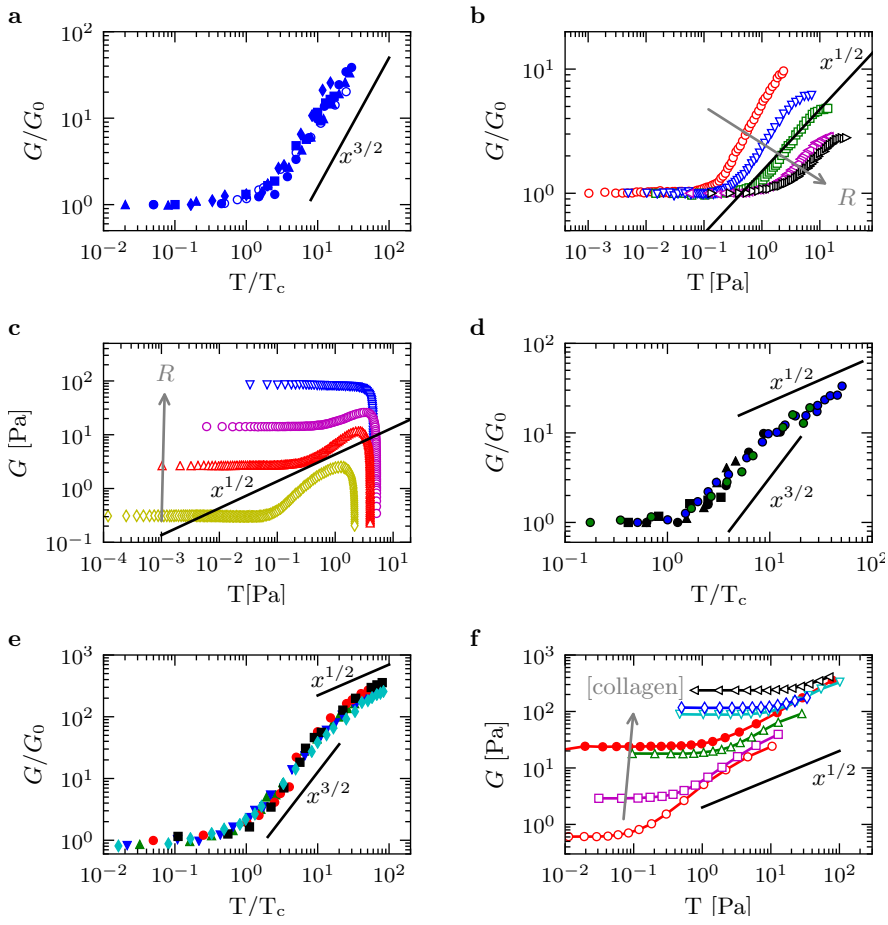

Figure 6.1. The nonlinear behavior of biopolymer networks plotted as the shear modulus G vs. stress T or the shear modulus normalised by the initial shear modulus G/G_0 vs. stress normalised by the critical stress at the onset of nonlinearity T/T$_c$ for: **a**, F-actin/scruin networks (Gardel et al., 2004a), **b**, F-actin/rigor-HMM networks with actin concentration 19 μM, mean F-actin length 21 μm and various increasing molar HMM/actin concentration ratios $R = c_{\mathrm{HMM}}/c_{\mathrm{a}}$ indicated by the arrow (Tharmann et al., 2007), **c**, bundled F-actin/fascin networks with actin concentration 0.4 mg/ml and various increasing molar facin/actin concentration ratios $R = c_{\mathrm{fascin}}/c_{\mathrm{a}}$ indicated by the arrow (Lieleg et al., 2007), **d**, F-actin/filamin networks for lower F-actin concentrations (Kasza et al., 2009), **e**, vimentin networks (Lin et al., 2010a), **f**, branched collagen I type networks, closed symbol (Lindstrom et al., 2010) and open symbol (Vader et al., 2009), with increasing collagen concentration indicated by the arrow.

described in § 2.2. In this chapter, we will use network RVE realizations generated for constant fibre concentration $c_f = 0.8\,\mathrm{mg/ml}$ and an initial fibre length $l_0 = 5\,\mu\mathrm{m}$. The box size is $W = 2.5\,\mu\mathrm{m}$ (Huisman et al., 2007). The stress-strain response of networks is obtained by subjecting the RVE to simple shear in a quasi-static finite element simulation, as described in § 2.3. In these computations, unless stated otherwise, the material parameters of the fibre beam elements are set to represent F-actin with stretching stiffness $\mu = 4 \times 10^{-8}\,\mathrm{N}$ (Liu and Pollack, 2002), bending stiffness $\kappa = 6.75 \times 10^{-26}\,\mathrm{Nm}^2$ (Ott et al., 1993) and a torsional stiffness that is equal to the bending stiffness. The mechanical behavior of cross-links is represented by simple linear springs, as described in § 2.4. The behavior of the cross-links is further simplified by coupling the four cross-link spring constants to a single parameter, the spring constant $s = s_1 = s_3 = s_2/l_c^2 = s_4/l_c^2$. The mean macroscopic stress (T) response to shear strain Γ is calculated as the ensemble average over seven to ten random RVE realizations at constant stress level. From this, the strain dependent ensemble averaged elastic shear modulus is obtained as $G = \partial \mathrm{T}/\partial\Gamma$.

6.2 Results and discussion

The cross-link number $\tilde{s}$, defined by $\tilde{s} = (sl_c^3)/\kappa$, is a measure of the cross-link stiffness relative to that of the fibre segment. It is not surprising to see in Figure 6.2a that the initial network response as a function of $\tilde{s}$ is reminiscent of the behavior of two "springs" connected in series. In the rigidly cross-linked limit (RCL), i.e. $\tilde{s} \to \infty$, the initial response is independent of $\tilde{s}$ and is fibre dominated. Moreover, the RCL network at small strains is a bending dominated structure, much like an open cell foam (Gibson and Ashby, 1997), with a linear dependence of the initial shear modulus G_0 on the fibre bending stiffness, $G_0 = G_0^\infty \propto \kappa$ (Žagar et al., 2011). For $\tilde{s}$ below the transition marked by $\tilde{s} = \tilde{s}_\kappa \approx 100$, the initial response is cross-link dominated with $G_0/G_0^\infty \propto \tilde{s}$, while G_0 is expected to vanish in the limit $\tilde{s} \to 0$ when force can no longer be transmitted through the network.

6.2.1 Bending dominated stiffening

Networks generally show a linear stress response at small strains, i.e. constant stiffness G up to a critical strain Γ_c or critical stress T_c, followed by nonlinear strain-stiffening at large strains (Figure 6.2b and Figure 6.2c). The behavior of RCL networks have been studied extensively in Chapter 5; here we just briefly summarise the main findings.

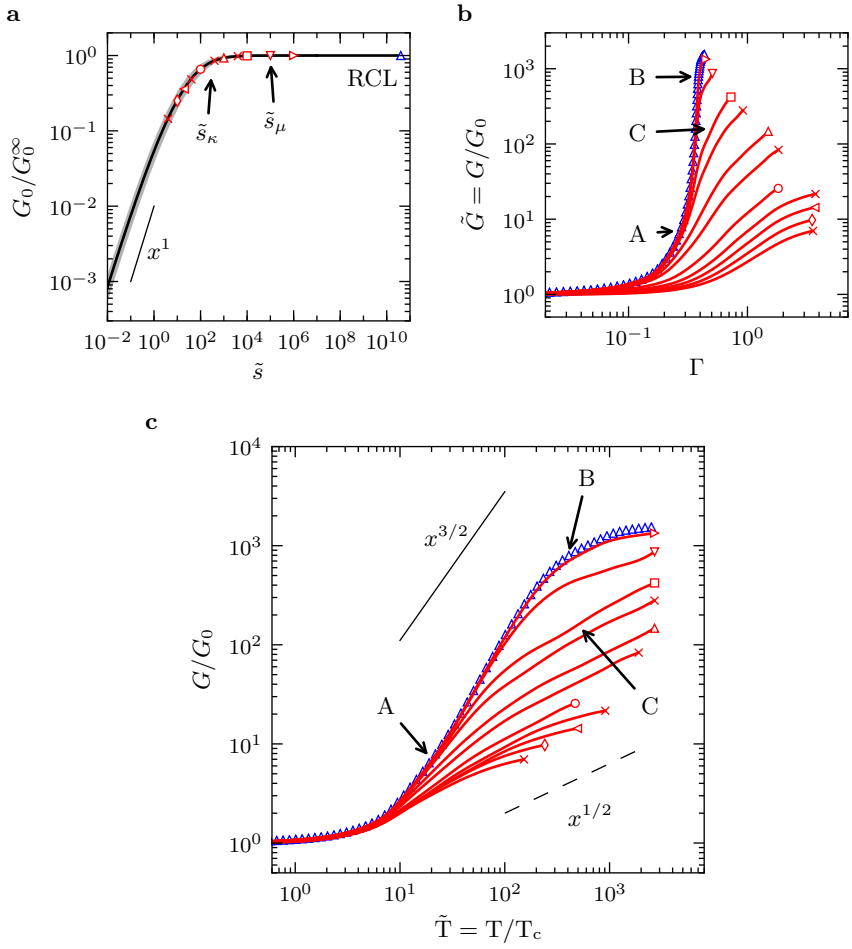

Figure 6.2. The effect of cross-link number $\tilde{s}$ of the networks with constant connectivity $\tilde{n}_\mathrm{X} \approx 0.34$, $l_\mathrm{c} \approx 0.86\,\mu$m. **a**, The ensemble averaged small strain response as a function of cross-link number $\tilde{s}$. The initial shear modulus G_0 is normalised by the initial network shear modulus in the rigidly cross-linked limit G_0^∞. The standard deviation is represented by the gray region. **b** and **c**, The ensemble averaged shear modulus $\tilde{G} = G/G_0$ as a function of strain Γ and normalised stress $\tilde{\mathrm{T}}$ for selected $\tilde{s}$ values as indicated by the symbols in panel a. The response of the RCL networks is shown in blue. The standard deviations (up to about twice the symbol size) are not shown.

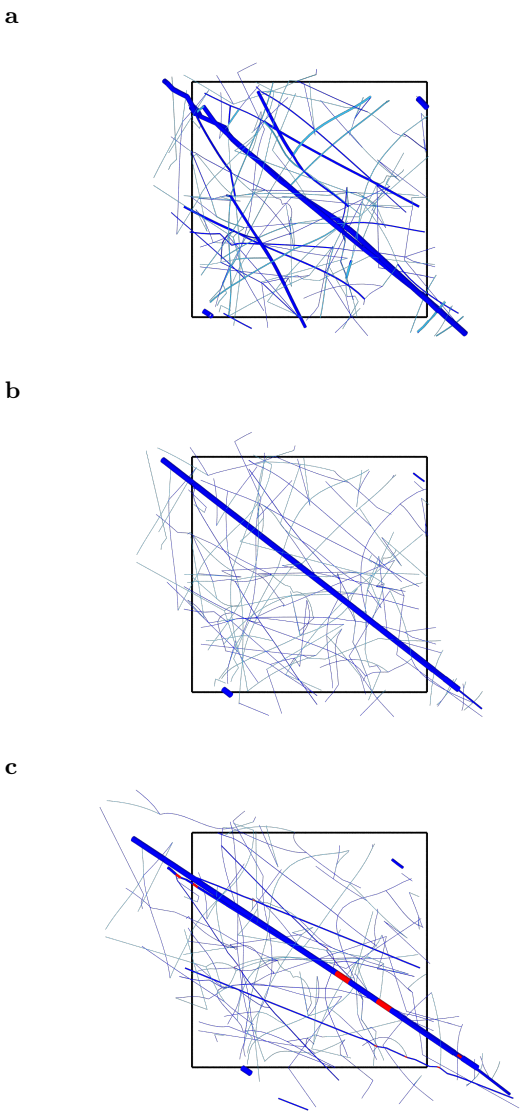

Figure 6.3. View of the deformed network at stress states indicated by letters in Figure 6.2b and Figure 6.2c for RCL case at **a**, $\tilde{\mathrm{T}} \approx 20$ and **b**, $\tilde{\mathrm{T}} \approx 400$, and **c**, $\tilde{\mathrm{T}} \approx 500$ at $\tilde{s} = 10^4$. The filaments in tension/compression are shown in blue/light-blue and cross-links in red. The thickness of the constituent corresponds to the normalised element axial force $|f_1^e / \max(f_1^e)|$.

RCL networks stiffen rapidly with a 3/2 power-law dependence of the normalised shear modulus $\tilde{G}$ on normalised stress $\tilde{\mathrm{T}} = \mathrm{T}/\mathrm{T_c}$ (Figure 6.2c, blue); the same phenomenology is observed in experiments on cross-linked F-actin/scruin (Gardel et al., 2004a,b) and neuro-filament networks (Lin et al., 2010b).

The deformed microstructures reveal that the 3/2 power-law stiffening is associated with the formation and subsequent stretching of an oriented stress path (appearing in thick lines, Figure 6.3a and Figure 6.3b). From the moment the percolating stress path emerges (i.e. at the critical strain Γ_c), continued shearing predominantly increases the axial stress of the sections in the path, while the path itself straightens-out and load transfer completely localises inside the path (Figure 6.3b). In contrast to the non-affine behavior of the network defining the initial network response, the nonlinear strain stiffening in a RCL network is dominated by the affine stretching of the localised stress path. The 3/2 stiffening behavior therefore, can be analysed in terms of a single stress path in a box (see Žagar et al. (2011) and Section §§ 6.2.3 for details). When considered independent from the rest of the network, the stress path can be seen as a statically undulated filament under tension, which has been shown (van Dillen et al., 2008) to exhibit the same asymptotic behavior as a thermally undulated semi-flexible chain in the MacKintosh model (MacKintosh et al., 1995; Storm et al., 2005). At high $\tilde{\mathrm{T}}$, due to the finite axial stiffness of the fibres, the network response becomes stretching dominated and linear again, but now with a modulus $\tilde{G} = \tilde{G}_\mu$ that scales with the axial stiffness μ.

6.2.2 Finite strain effect

By decreasing the cross-link stiffness from the RCL limit, the network response starts to become affected significantly at the moment when stretching of the cross-links in the path at high $\tilde{\mathrm{T}}$ becomes as favorable as stretching of the fibre sections; this occurs when $s \approx \mu/l_c$ or equivalently $\tilde{s} \approx \tilde{s}_\mu = \mu l_c^2/\kappa$ (open down triangle, Figure 6.2c). Below $\tilde{s}_\mu$, we observe that the network shear modulus at high $\tilde{\mathrm{T}}$, instead of becoming constant $\tilde{G}_\mu$, transits to a novel power law $\tilde{G} \propto \tilde{\mathrm{T}}^{1/2}$ (open triangle, Figure 6.2c). Interestingly, power-law stiffening with an exponent near 1/2 has been observed in experiments for various biopolymer networks, as shown in Figure 6.1 (Tharmann et al., 2007; Lindstrom et al., 2010; Vader et al., 2009; Kasza et al., 2009; Gardel et al., 2006; Lin et al., 2010a).

The 1/2 power-law region continues to be dominated by the mechanics of a stress path (Figure 6.3c), although now, the axial stiffness of the path is controlled by the cross-links (elements shown in red). Since the stiffness of the stress path is much smaller now than that of the fibre sections, the shear strains can become

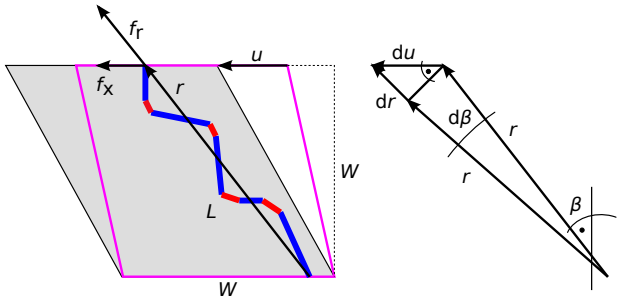

Figure 6.4. Simple shear of the box containing a percolating stress path. The box at the critical point is shown in magenta. Filament constituent is shown in blue and cross-links in red.

larger (Figure 6.2b), giving raise to an enhanced reorientation of the stress path. In the subsequent section we will show that a simple model of a stress path in a box can explain both this 1/2 scaling and the 3/2 scaling for RCL networks.

6.2.3 Stress path in a box

We idealise the nonlinear behavior of a network containing a stiffening stress path as that of a single fibre of filament sections and cross-links in a cubic box of length W, see Figure 6.4. This nonlinear stress path is assumed to emerge under shear at a critical stress level $\mathrm{T_c}$ with corresponding strain Γ_c. Beyond this strain, the initially constant stiffness G_0 abruptly changes into a stiffness that depends on the relative strain $\gamma := \Gamma - \Gamma_c$. In order to derive this function $G(\gamma)$, we first observe that the shear stress can simply be expressed in terms of the end-to-end force f_r on the stress path: $\mathrm{T} = f_r \sin\beta / W^2$. Here, $\beta = \arctan\Gamma$ is the instantaneous orientation of the end-to-end vector as indicated in Figure 6.4. The force in the stress path varies with strain as the end-to-end vector changes both in length and orientation. The change of the length r of the end-to-end vector can be expressed as $\mathrm{d}r = \mathrm{d}u\ \sin\beta = W\mathrm{d}\Gamma\ \sin\beta$ by simple geometrical considerations. Keeping the strain dependence of r and β in mind, we thus find that the instantaneous stiffness satisfies

$$G = \frac{\mathrm{dT}}{\mathrm{d}\Gamma} \propto \sin\beta \frac{\mathrm{d}}{\mathrm{d}r}\left(f_r \sin\beta\right) . \tag{6.1}$$

Interesting scaling relations between G and γ can be found by considering two limiting situations.

The first limiting case is the RCL network. Such a network has been observed

to stiffen so rapidly that $\gamma \approx 0$, so that β remains roughly constant at the critical value β_c. As a consequence, from (6.1), $G \propto \mathrm{d}f_r/\mathrm{d}r$. The stress path in this case consists of an athermal yet undulated filament, which rapidly stiffens when its length r approaches its contour length L. In fact (van Dillen et al., 2008), the force f_r in inextensible filaments diverges as $(L-r)^{-2}$ when $r \to L$. Hence, $G \propto (L-r)^{-3}$ or $G \propto \mathrm{T}^{3/2}$. The stiffness of extensible filaments does not diverge but is limited to the axial stiffness μ. Thus, $G \propto \mu$ defines an upper limit to the validity of the above 3/2 scaling law.

When the cross-link compliance is significant, networks are more easily deformed to larger strains (Figure 6.2b) and the reorientation of the stress path during stiffening can be substantial. β can surpass the critical orientation $\beta_c = \arctan \Gamma_c$. With both f_r and β being dependent on strain, (6.1) can be expanded to read

$$G \propto \sin^2\beta \frac{\mathrm{d}f_r}{\mathrm{d}r} + \cos^2\beta \frac{f_r}{r}\,. \tag{6.2}$$

In the regime that $s \ll \mu/l_c$ (equivalent to $\tilde{s} \ll \tilde{s}_\mu$) yet $s \gg \kappa/{l_c}^3$ (equivalent to $\tilde{s} \gg 1$), the overall response of the composite stress path can be approximated as being bi-linear. Initially, the composite path force-displacement response would be filament dominated so that its slope is proportional to $\kappa/{l_c}^3$. Beyond the critical point however, i.e. at high tension, the response is linear and cross-link dominated thus, the slope is proportional to s, as observed in Figure 6.3c. Since $s \gg \kappa/{l_c}^3$, beyond the critical point then holds that $\mathrm{d}f_r/\mathrm{d}r \gg f_r/r$, and the last term in (6.2) can be neglected, yielding

$$G \propto \sin^2\beta \frac{\mathrm{d}f_r}{\mathrm{d}r}\,. \tag{6.3}$$

With $\mathrm{d}f_r/\mathrm{d}r \propto s$, what remains is to find the relationship between $\sin^2\beta$ and γ. In order to be able to cast this in a simple form, we will consider small excursions into the nonlinear regime, so that $\beta - \beta_c$ is small. Then, we set $\cos\beta \approx \cos\beta_c$ so that $\sin\beta$ can be developed as $\sin\beta = \tan\beta\cos\beta_c = (\tan\beta_c + \gamma)\cos\beta_c = \sin\beta_c + \gamma\cos\beta_c$. The two leading terms in the expansion of (6.3) thus become

$$G \propto s(1 + b\gamma)\,,$$

with b being determined solely by the critical orientation and having a value of order one. Writing the bracketed term as $y = 1 + b\gamma$, we find that $G = \mathrm{d}\mathrm{T}/\mathrm{d}\Gamma = \mathrm{d}\mathrm{T}/\mathrm{d}\gamma = \mathrm{d}\mathrm{T}/\mathrm{d}y$ leads to the differential equation $\mathrm{d}\mathrm{T} \propto sy\mathrm{d}y$. Its solution $\mathrm{T} \propto sy^2$ allows us to write $G \propto y$ or $G \propto \mathrm{T}^{1/2}$ for cross-link dominated stiffening.

According to the derivation above, a power-law dependence of instantaneous modulus on stress with exponent 1/2 is expected when the nonlinear strain γ is

small enough that the dependence of the re-orientation of the stress path on γ is linear. The nonlinear effects at large strains are expected to push the exponent away from 1/2 towards a constant stiffness of $G \propto s$.

6.2.4 Effect of connectivity $\tilde{n}_\mathrm{X}$

In experiments where the concentration of cross-linking molecules is varied at a constant fibre concentration and at a constant fibre length, it has been found that if the concentration of cross-linking molecules increases, the stiffening of the network decreases (cf. Figure 6.1b, c and f). The explanation for this, however, is elusive. Since an increase in the concentration of the cross-linking molecule is expected to increase the network connectivity, in this section the effect of connectivity on the nonlinearity of the network response is investigated via the cross-link number $\tilde{s}$.

First note that for constant l_0, $\tilde{n}_\mathrm{X}$ is directly related to the mean cross-link spacing l_c (see Chapter 3), which in turn is key in the balance between cross-link and filament stiffness as expressed by $\tilde{s} = s l_\mathrm{c}^3/\kappa$. As a consequence, by varying $\tilde{n}_\mathrm{X}$ in Figure 6.5 from 0.12 to 0.72, at fixed l_0 and at fixed cross-link spring constant $s \approx 4 \times 10^{-5}\,\mathrm{N/m}$ (lines shown in green), we effectively change the value of $\tilde{s}$ by nearly two orders of magnitude. The cross-link spring constant s is chosen such that for moderate connectivity $\tilde{n}_\mathrm{X} \approx 0.34$ and $l_\mathrm{c} \approx 0.86\,\mu\mathrm{m}$ (triangle), $\tilde{s}_{0.34}$ is in the knee of the transition seen in Figure 6.2a, $\approx \tilde{s}_\kappa$. At this connectivity, the small strain behaviour is dominated by the bending of the fibre sections, since $G_0/G_0^\infty \approx 1$, while the nonlinear behaviour is governed only by the finite strain effect (1/2 power-law stiffening), as seen previously in Figure 6.2c.

The network with low connectivity $\tilde{n}_\mathrm{X} \approx 0.12$ (green circle) has longer fibre sections ($l_\mathrm{c} = 1.2\,\mu\mathrm{m}$) than for $\tilde{n}_\mathrm{X} \approx 0.34$, and due to the decreased relative bending rigidity, the cross-link number $\tilde{s}_{0.12}$ increases above $\tilde{s}_{0.34}$. The response for $\tilde{n}_\mathrm{X} \approx 0.12$ therefore starts as in the RCL limit and is followed by the nonlinear behavior that is initially dominated by 3/2 stiffening. At increased stress however, the response undergoes a bending-to-stretching transition after which stiffening behavior is governed by the 1/2 mechanism, as is expected for $\tilde{s} > \tilde{s}_\kappa$. For networks with $\tilde{n}_\mathrm{X} \approx 0.72$ (green square) on the other hand, this effect is reversed: a short section length ($l_\mathrm{c} \approx 0.34\,\mu\mathrm{m}$) increases the bending rigidity of fibre sections, so that $\tilde{s}_{0.72} < \tilde{s}_{0.34}$. Thus, such networks are initially softer than in the RCL limit (blue square) and exhibit 1/2 stiffening.

The effect of connectivity on $\tilde{s}$ and the network response presented in Figure 6.5 nicely explains the trends observed in experiments with F-actin/rigor-HMM networks (Tharmann et al., 2007) (Figure 6.1b). The decreasing stiffening behavior observed for increasing HMM concentration at constant concentration of F-actin

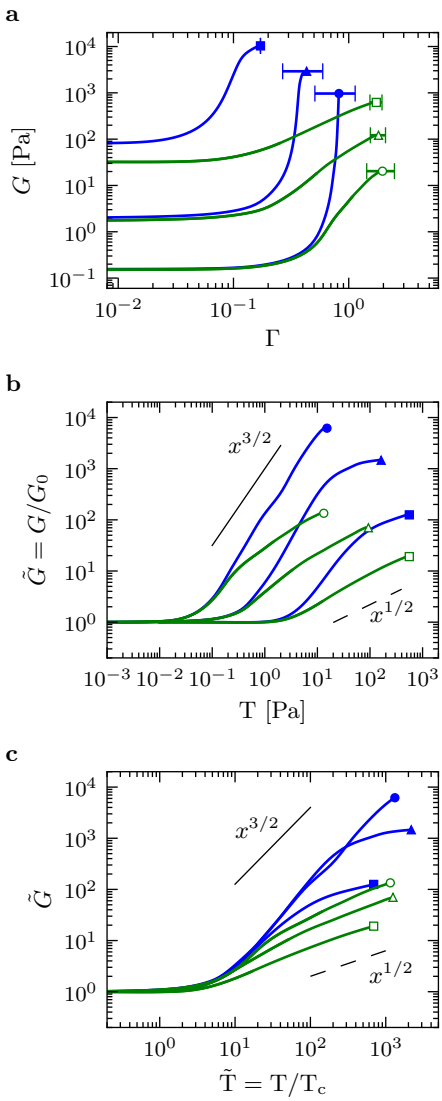

Figure 6.5. The effect of connectivity $\tilde{n}_{\mathrm{X}}$. The ensemble averaged response: **a**, $G(\Gamma)$, **b**, $\tilde{G}(\mathrm{T})$ and **c**, $\tilde{G}(\tilde{\mathrm{T}})$ of networks for cross-link spring constants: $s \to \infty$ (blue) and $s \approx 4 \times 10^{-5}\,\mathrm{N/m}$ (green) and connectivity: $\tilde{n}_{\mathrm{X}} \approx 0.12$, $l_{\mathrm{c}} \approx 1.2\,\mu\mathrm{m}$ (○), $\tilde{n}_{\mathrm{X}} \approx 0.34$, $l_{\mathrm{c}} \approx 0.86\,\mu\mathrm{m}$ (△) and $\tilde{n}_{\mathrm{X}} \approx 0.72$, $l_{\mathrm{c}} \approx 0.34\,\mu\mathrm{m}$ (□). The standard deviations (up to about twice the symbol size) are not shown.

and constant F-actin length naturally emerges from a decreasing $\tilde{s}$, which in turn shifts the network response from the 3/2 mechanism towards the 1/2 mechanism (Figure 6.5b and Figure 6.5c). It is interesting to note that, since $\tilde{s} \approx \tilde{s}_\kappa$ for F-actin/rigor-HMM networks, they behave only as rigidly cross-linked networks at small strains and for lower rigor-HMM concentrations. A similar argument for the reduction of $\tilde{s}$ upon increased connectivity can be applied to bundled F-actin/fascin networks (Lieleg et al., 2007) (Figure 6.1c) as well as to branched networks of collagen I type (Vader et al., 2009; Lindstrom et al., 2010) (Figure 6.1f), albeit in terms of branching rather than cross-linking.

6.2.5 Characteristic ratio

As shown in sub-section §§ 6.2.3, the stiffening behavior of the cross-linked networks can be understood in terms of the response of a single stress path. For RCL networks, the stress path comprises only fibre sections so that the dependence of the response on the fibre properties μ and κ can be conveniently related to the characteristic ratio $l_\mathrm{b}/l_\mathrm{c}$, where $l_\mathrm{b} = \sqrt{\kappa/\mu}$ (note that for a homogeneous beam with a circular cross-section, l_b is equal to the half of the beam radius).

In Figure 6.6 we demonstrate how the response of a RCL network depends on the characteristic length l_b. For this, we use a single microstructure with fixed $l_\mathrm{c} = 0.86\,\mu\mathrm{m}$, which was shown in Figure 6.3a. The response for fibre properties set to represent F-actin, e.g. $\mu = \mu_\mathrm{a} = 4 \times 10^{-8}\mathrm{N}$ and $\kappa = \kappa_\mathrm{a} = 6.75 \times 10^{-26}\mathrm{Nm}$, in Figure 6.6 is indicated by the star. Since in this case $l_\mathrm{b}/l_\mathrm{c} \approx 1/1000 \ll 1$, networks with larger ratios $l_\mathrm{b}/l_\mathrm{c}$ than RCL F-actin are obtained for $\mu < \mu_\mathrm{a}$ and constant $\kappa = \kappa_\mathrm{a}$ (magenta full symbols) or for $\kappa > \kappa_\mathrm{a}$ and constant $\mu = \mu_\mathrm{a}$ (blue open symbols).

As expected, the small strain response of the RCL network in Figure 6.6a is bending dominated with $G_0 \propto l_\mathrm{b}^2$, or $G_0 \propto \kappa$ for $l_\mathrm{b}/l_\mathrm{c} \ll 1$ and stretching dominated with $G_0 \propto l_\mathrm{b}^{-2}$ or $G_0 \propto \mu$ when $l_\mathrm{b}/l_\mathrm{c} \to 1$. The response at large strains becomes increasingly less nonlinear for increasing $l_\mathrm{b}/l_\mathrm{c}$ (Figure 6.6b) with a clearly observable 3/2 to 1/2 stiffening transition (Figure 6.6c). In addition, the different responses corresponding to the same magnitude of $l_\mathrm{b}/l_\mathrm{c}$ (e.g. open and closed symbols in Figure 6.6b and Figure 6.6c), are indentical, indicating that the ratio $l_\mathrm{b}/l_\mathrm{c}$ is the key parameter to characterise the response of a RCL network, just like the spring number $\tilde{s}$ for the cross-linked networks in Figure 6.2 and Figure 6.5. Essentially, the same trends previously observed in Figure 6.2c for cross-linked networks in terms of the spring number $\tilde{s}$ are now confirmed in Figure 6.6c for RCL networks in terms of $l_\mathrm{b}/l_\mathrm{c}$.

In general, the stress path of cross-linked network comprises fibre sections and

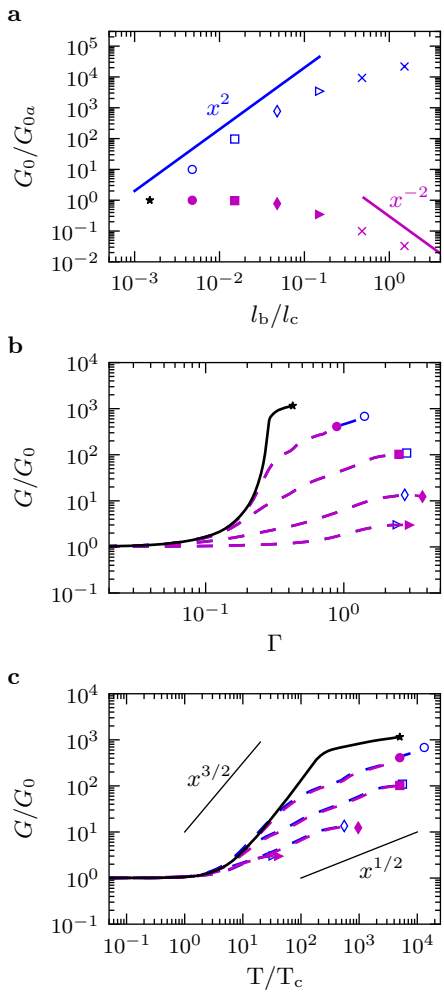

Figure 6.6. **a**, The normalised initial shear modulus G_0/G_{0a} of the RCL network with $l_c = 0.86\,\mu$m vs. characteristic ratio l_b/l_c, where G_{0a} is the initial shear modulus calculated for the RCL F-actin network with $\mu = \mu_a = 4 \times 10^{-8}$N and $\kappa = \kappa_a = 6.75 \times 10^{-26}$Nm. The l_b/l_c for the RCL F-actin network corresponds to a star. Different ratios l_b/l_c larger than the F-actin network are obtained either for $\mu < \mu_a$ and constant $\kappa = \kappa_a$ (magenta full symbols) or for $\kappa > \kappa_a$ and constant $\mu = \mu_a$ (blue open symbols). **b** and **c**, The large strain response of the RCL network for various ratios l_b/l_c shown in panel **a**, where G/G_0 is the network shear modulus scaled by the initial modulus G_0 and T/T$_c$ is the stress scaled by the stress value at the onset of nonlinearity T$_c$.

cross-links in series so that its "effective" compliance can be estimate to be the sum of those of the fibres and of the cross-links. Thus, we generalise the characteristic ratio of the composite stress path as $\bar{l}_\mathrm{b}/l_\mathrm{c} = \sqrt{k_\mathrm{b}/k_\mathrm{a}}$, with the effective bending spring constant $k_\mathrm{b} \approx 1/(l_\mathrm{c}^3/\kappa + 1/s)$ and the effective axial spring constant $k_\mathrm{a} \approx 1/(l_\mathrm{c}/\mu + 1/s)$. The resulting effective ratio $\bar{l}_\mathrm{b}/l_\mathrm{c}$ can thus be written as

$$\frac{\bar{l}_\mathrm{b}}{l_\mathrm{c}} \approx \sqrt{\frac{\tilde{s}(l_\mathrm{b}/l_\mathrm{c})^2 + 1}{\tilde{s} + 1}}. \tag{6.4}$$

In the RCL limit where $\tilde{s} \gg 1$, $\bar{l}_\mathrm{b}/l_\mathrm{c} \to l_\mathrm{b}/l_\mathrm{c}$. On the other hand, for networks with constant filament constituents ($l_\mathrm{b}/l_\mathrm{c} = \text{const.}$), like the networks studied in Figure 6.2 and Figure 6.5, the characteristic ratio $\bar{l}_\mathrm{b}/l_\mathrm{c}$ can be uniquely related to the cross-link number $\tilde{s}$. For example, for networks with $l_\mathrm{b}/l_\mathrm{c} \ll 1$ and cross-link number $1 \ll \tilde{s} \ll \tilde{s}_\mu$ (see Figure 6.2), the expression (6.4) suggests an inverse square root dependence, i.e. $\bar{l}_\mathrm{b}/l_\mathrm{c} \approx 1/\sqrt{\tilde{s}}$. In addition, note that a small characteristic ratio $\bar{l}_\mathrm{b}/l_\mathrm{c} \ll 1$ leads to the bending dominated stiffening mechanism and network behavior characterized by the power law $\tilde{G} \propto \tilde{\mathrm{T}}^{3/2}$. For higher characteristic ratios the network large strain behavior is showing a transition to stretching dominated stiffening, characterized by the power-law exponent 1/2.

The importance of (6.4) is that it generalises the parameters $\tilde{s}$ and $l_\mathrm{b}/l_\mathrm{c}$ to $\bar{l}_\mathrm{b}/l_\mathrm{c}$. With this, the large-strain response of a cross-linked network can be characterised by a single parameter $\bar{l}_\mathrm{b}/l_\mathrm{c}$, as demonstrated in Figure 6.7. This graph of normalised shear modulus G/G_0 vs. normalised stress $\mathrm{T}/\mathrm{T}_\mathrm{c}$ can serve as a master plot, which based on the value of $\bar{l}_\mathrm{b}/l_\mathrm{c}$ uniquely defines the two critical points of the response: the strain Γ_c (or stress T_c) at the onset of nonlinearity and the bending-to-stretching stiffening mechanism transition.

The precise determination of k_a and k_b of a composite stress path and the corresponding $\bar{l}_\mathrm{b}/l_\mathrm{c}$, however, requires detailed knowledge of the composition of the stress path: the number of fibre sections and cross-links in the path as well as their connectivity. Thus, in order to correctly identify the network master curve as a function of $\bar{l}_\mathrm{b}/l_\mathrm{c}$, these details should be accounted for. Unfortunately, this information is generally difficult to obtain, since the stress path forms only after the network response passes its critical point and becomes nonlinear. Moreover, it can be expected that the stress path composition is influenced by the concentration of the network constituents and the network microstructure, and this dependence is not yet known.

Additional complications in evaluating the effective spring constants k_a and k_b arise from the fact that the load-bearing network structure sometimes is more complex than a single stress path, as shown, for example, in Figure 6.8. Commonly,

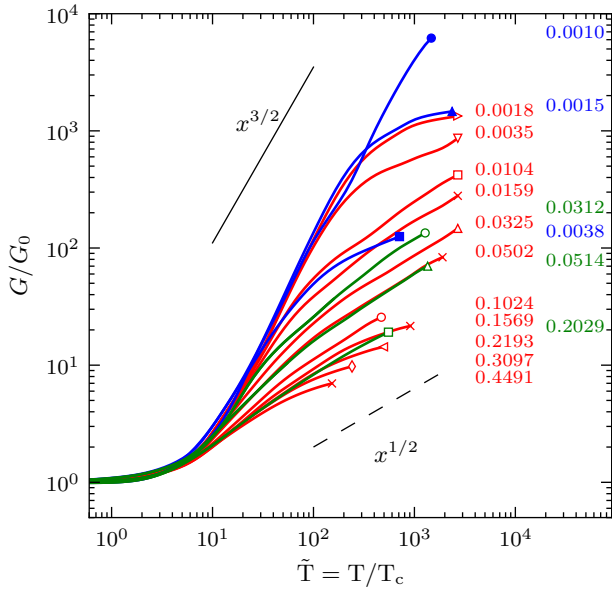

Figure 6.7. Compilation of all curves of G/G_0 vs. normalised stress T/T_c, along with the corresponding values of $\bar{l}_b/l_c$, for the cases in Figure 6.2c (where cross-link stiffness is varied at constant connectivity) and Figure 6.5c (at constant cross-link stiffness but varying connectivity), respectively.

these kinds of supportive frames are found in networks of larger connectivity (Figure 6.8a and Figure 6.8b), but they can also be observed in low to moderately connected networks when they have very compliant cross-links (Figure 6.8c). Similar supportive frames have also been observed in molecular dynamics simulations of F-actin networks by Kim et al. (2009b). Despite the difference in appearance, however, supportive frames are qualitatively not different from individual stress paths. For example, the RCL network with a high connectivity of $\tilde{n}_X \approx 0.72$, whose supportive frame is shown in Figure 6.8a, stiffens according to a 3/2 power law (blue square Figure 6.5b), but if the cross-links are compliant, the stiffening of the same network follows a 1/2 power law (red open square Figure 6.8b) despite the fact that the corresponding supportive frames are very different (see Figure 6.8b). These results suggest that a supportive frame consists of a set of several stress paths interconnected in series or in parallel, as directly suggested by Figure 6.8. Hence, the specific architecture of a supportive frame is expected to affect only the magnitudes in the response but not the general scaling relations.

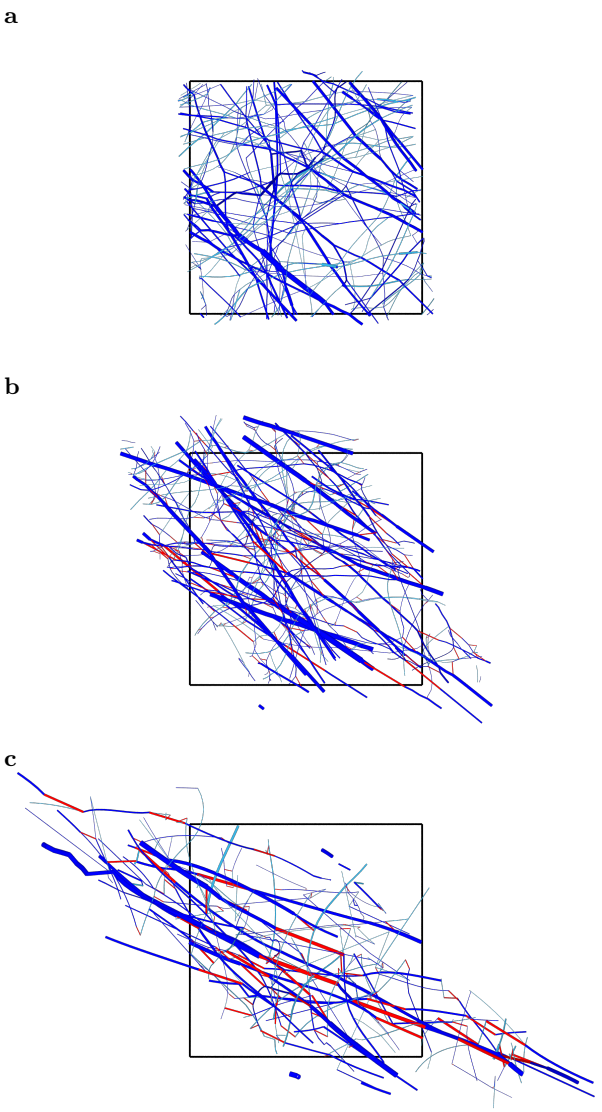

Figure 6.8. View through the deformed network realization showing load bearing supportive frames: **a**, $\tilde{n}_X \approx 0.72$ for RCL limit in Figure 6.5 (blue square) at $T \approx 30\,\mathrm{Pa}$, **b**, $\tilde{n}_X \approx 0.72$ for $s \approx 4e - 5\,\mathrm{N/m}$ in Figure 6.5, (green square) at $T \approx 65\,\mathrm{Pa}$, **c**, $\tilde{n}_X \approx 0.34$ for $\tilde{s} = 10$ in Figure 6.2, (red diamond) at $\tilde{T} \approx 30$. The axial stress map is obtained in the same way as in Figure 6.3.

6.3 Conclusions

In this chapter a detailed investigation has been performed of the structure-property relations of a discrete 3D random network of cross-linked fibres, relating the stiffening behavior to the material properties of its constituents and the network microstructure.

The observation that the nonlinear network response is dominated by the behavior of a localised percolating path across axially stressed network constituents allows for a simple rationalization of the strain-stiffening behavior in terms of two fundamental mechanisms: (i) the pulling-out of stress path undulations and (ii) finite strain effects induced by reorientation of the stress path. While the first of these is a bending-dominated mechanism that can be characterised by a power-law dependence with exponent 3/2 of the shear modulus $\tilde{G}$ on stress $\tilde{\mathrm{T}}$, the second has been disclosed here as a stretching-dominated finite strain effect that gives rise to a power-law relation between $\tilde{G}$ and $\tilde{\mathrm{T}}$ with exponent 1/2.

The characteristic ratio $\bar{l}_\mathrm{b}/l_\mathrm{c}$ has been shown to control the nonlinear strain-stiffening ability of a cross-linked network, both in determining the critical point for the onset of nonlinearity and the bending-to-stretching stiffening transition. Since $\bar{l}_\mathrm{b}/l_\mathrm{c}$ relates material properties (bending and axial stiffnesses) of the network constituents to the key length scale of the microstructure (l_c), the same network response can be obtained in various ways for different networks. This unification of large strain behaviour has been demonstrated in the form of master plots of normalised shear modulus G/G_0 against normalised stress $\mathrm{T}/\mathrm{T}_\mathrm{c}$ for different $\bar{l}_\mathrm{b}/l_\mathrm{c}$.

A bending dominated response at large strains leading to 3/2 power-law stiffening is pronounced for $\bar{l}_\mathrm{b}/l_\mathrm{c} \ll 1$. Such strain-stiffening behavior is governed by a much larger axial stiffness of the developed stress path in the network relative to the stress path effective bending properties. Examples of networks that stiffen in this way all the way up to fracture are F-actin/scruin networks (Gardel et al., 2004a,b) and cross-linked neuro-filaments (Lin et al., 2010b) (Figure 6.1a).

Surprisingly, however, not many biopolymer networks exhibit stiffening behavior characterized by such low $\bar{l}_\mathrm{b}/l_\mathrm{c}$. Networks associated with a somewhat higher characteristic ratio, e.g. $\bar{l}_\mathrm{b}/l_\mathrm{c} \approx 0.01$, show a transition from 3/2 to 1/2 power-law stiffening, such as the F-actin/filamin networks in Figure 6.1d or the intermediate filament networks in Figure 6.1e. However, due to rupture in real networks, it might be difficult to distinguish the transition between the stiffening mechanisms from convergence towards the maximum network stiffness. This upper limit is likely to be determined by the effective axial stiffness $G \propto 1/(l_\mathrm{c}/\mu + 1/s)$.

For networks with $\bar{l}_\mathrm{b}/l_\mathrm{c} \approx 0.1$, the large strain response is mainly dominated by the stretching mechanism, leading to stiffening with a power-law exponent

1/2. Such increased characteristic ratios $\bar{l}_b/l_c$ can arise in networks from rather compliant filament inter-connections, e.g cross-linking molecules in the case of F-actin/rigor-HMM (Tharmann et al., 2007) (Figure 6.1b), or collagen branching points in the case of branched collagen I type networks (Lindstrom et al., 2010; Vader et al., 2009) (Figure 6.1f).

For networks with $\bar{l}_b/l_c \to 1$, the stiffening ability is greatly diminished due to the 1/2 mechanism, while the onset of nonlinearity is being pushed to larger strains. Such trends can be observed in bundled F-actin/fascin networks (Figure 6.1c) at high fascin concentrations, where networks are found to be unable to stiffen at all. In these networks, a higher fascin concentration can increase the bending resistance of the bundles in several simultaneous ways, e.g. by decreasing the length of the bundle segments (equivalent to l_c in our model), by increasing the bundle diameter (Lieleg et al., 2007) and by increasing the coupling between the filaments within the bundle (Claessens et al., 2006). Thus, a higher fascin concentration could increase $\bar{l}_b/l_c$ to values ~ 1 and cause network rupture long before the finite strain effect can give rise to stiffening.

In conclusion, various biopolymer networks of different constituents and different microstructures show strain-stiffening trends that can be understood in terms of the competition between two stiffening mechanisms. The relative importance of the two mechanisms in the stiffening response can be expressed through the effective characteristic ratio $\bar{l}_b/l_c$ of the network. The strain-stiffening trends observed experimentally in a wide variety of biopolymer networks thus becomes unified in this single parameter.